Clustering of Particles Falling in a Turbulent Flow

K. Gustavsson, S. Vajedi, and B. Mehlig
Department of Physics, Gothenburg University, 41296 Gothenburg, Sweden
(Received 2 January 2014; published 29 May 2014)

Spatial clustering of identical particles falling through a turbulent flow enhances the collision rate between the falling particles, an important problem in aerosol science. We analyze this problem using perturbation theory in a dimensionless parameter, the so-called Kubo number. This allows us to derive an analytical theory quantifying the spatial clustering. We find that clustering of small particles in incompressible random velocity fields may be reduced or enhanced by the effect of gravity (depending on the Stokes number of the particles) and may be strongly anisotropic.

DOI: 10.1103/PhysRevLett.112.214501 PACS numbers: 47.55.Kf, 05.40.−a, 05.60.Cd, 47.27.eb

Particles suspended in an incompressible turbulent flow may cluster together even though direct interactions between the particles are negligible. This phenomenon is due to the inertia of the particles. It has been studied extensively in experiments [1–3] (see Ref. [4] for a review), in direct numerical simulations (DNS) [5–8], in model simulations [9], and by theoretical approaches [10–14]. In most DNS, model simulations, and theoretical studies of clustering, the effect of gravity is neglected. Those DNS that incorporate gravity tend to show that clustering is weakened when gravity causes the particles to fall through the flow [15–19]. But it has also been reported that gravity may increase clustering of particles falling through a turbulent flow [19], see also Ref. [15].

Clustering is commonly explained to be due to the fact that inertia allows the suspended particles to spiral out from vortices and gather in straining regions of the flow ("Maxey centrifuge effect" [10]). This mechanism was derived assuming that the inertia of the particles is not too large; their Stokes number $\mathrm{St} \equiv 1/(\gamma\tau)$ must be small. Here γ is the Stokes drag coefficient and τ is the smallest characteristic time scale of the flow (the Kolmogorov time in turbulent flows). Even though the fluid-velocity field is incompressible, the particle-velocity field acquires a degree of compressibility due to this effect. The strength of spatial clustering is determined by the divergence of the particle-velocity field. Since the explicit dependence upon the gravitational acceleration $\boldsymbol{g}$ drops out when this divergence is taken, it is argued that gravity does not affect clustering when St is small. But gravitational settling affects the fluctuations of the flow-velocity gradients seen by the falling particles. In particular, if the gravity parameter [20] $F \equiv |\boldsymbol{g}|\tau/u_0$ is large enough (u_0 is the Kolmogorov speed), then gravity pulls particles through the vortices. How does this affect the spatial clustering of the falling particles? Do the particles have time to spiral out from the vortices, or is the Maxey effect destroyed? What happens at larger St where "preferential sampling" in the absence of gravity is strong, but the particle positions are less correlated with the straining regions of the flow? How can we explain and quantify the anisotropy in the spatial patterns introduced by gravity (Fig. 1)? Finally, the inertial-particle dynamics exhibits "caustics" [21,22] where the phase-space manifold that describes the position dependence of the particle velocities folds over. This gives rise to large velocity differences between close-by particles [23–28]. How is the rate of caustic formation affected by gravity? These open questions are of crucial importance for the process of rain initiation in warm turbulent rain clouds [29,30].

In order to answer these questions and to quantify the degree of clustering of particles falling through a turbulent flow we analyze a model system: particles subject to gravity in a random velocity field in two spatial dimensions (see Ref. [14] and the caption of Fig. 1). We expect no essential difference in three dimensions. The model has three dimensionless parameters: St, F, and Ku. The Kubo number $\mathrm{Ku} \equiv u_0\tau/\eta$ (η is the smallest characteristic length scale of the flow) is a dimensionless correlation time. In this Letter we show how to compute the dynamics of the falling particles perturbatively, taking into account recursively that the perturbations due to the flow velocity cause the actual particle trajectory to deviate from its deterministic path. This yields an expansion in Ku [14,31,32], and results in

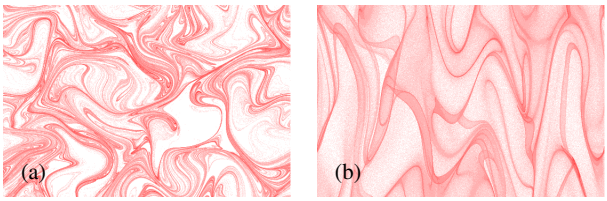

FIG. 1 (color online). Density of particles falling in a two-dimensional random velocity field $\boldsymbol{u}(\boldsymbol{r},t) = \nabla\psi(\boldsymbol{r},t) \times \hat{\boldsymbol{e}}_3$ in the negative y direction according to Eq. (1). Here $\hat{\boldsymbol{e}}_3$ is a unit vector orthogonal to the plane, and ψ is a Gaussian random function with zero mean and $\langle\psi(\boldsymbol{r},t)\psi(\boldsymbol{0},0)\rangle = (u_0^2\eta^2/2)\exp[-|t|/\tau - \boldsymbol{r}^2/(2\eta^2)]$. White (red) regions show low (high) particle densities. Size of the area shown: $10\eta \times 7\eta$. Parameters: $\mathrm{Ku} = 1, F = 1, \mathrm{St} = 0.2$ (a) and $\mathrm{St} = 10$ (b).

analytical expressions for the degree of clustering and its anisotropy as functions of St, F, and Ku. Neglecting effects due to finite particle size, we model the dynamics of a particle as

$$\dot{\boldsymbol{r}} = \mathrm{Ku}\boldsymbol{v}, \qquad \dot{\boldsymbol{v}} = [\boldsymbol{u}(\boldsymbol{r},t) - \boldsymbol{v}]/\mathrm{St} + F\hat{\boldsymbol{g}}. \tag{1}$$

Here dots denote total time derivatives (d/dt), $\boldsymbol{r}$ and $\boldsymbol{v}$ are particle position and velocity, $\boldsymbol{u}(\boldsymbol{r},t)$ is the fluid velocity evaluated at the particle position, and $\hat{\boldsymbol{g}} \equiv \boldsymbol{g}/|\boldsymbol{g}|$ points in the negative y direction. In Eq. (1) time, space, and speed scales are dedimensionalized by the characteristic scales τ, η, and u_0 of the flow.

Preferential sampling is characterized by the divergence $\nabla \cdot \boldsymbol{v}$ of the particle-velocity field. We compute the time average of $\nabla \cdot \boldsymbol{v}$ in terms of the matrix $\mathbb{Z}$ of the particle-velocity gradients $Z_{ij} \equiv \partial v_i/\partial r_j$ [11,13,14]. The dynamics of $\mathbb{Z}$ follows from Eq. (1): $\dot{\mathbb{Z}} = \mathrm{St}^{-1}(\mathbb{A} - \mathbb{Z}) - \mathrm{Ku}\mathbb{Z}^2$, and the effect of gravity is implicit in the dynamics of the matrix $\mathbb{A}$ of fluid-velocity gradients with elements $A_{ij} \equiv \partial u_i/\partial r_j$ evaluated along particle trajectories. To compute the dynamics of $\mathbb{A}(\boldsymbol{r}_t,t)$ along a particle trajectory $\boldsymbol{r}_t$, we expand around the deterministic ($\boldsymbol{u} = \boldsymbol{0}$) solution $\boldsymbol{r}_t^{(d)}$ of Eq. (1),

$$\boldsymbol{r}_t^{(d)} = \boldsymbol{r}_0 + \mathrm{Ku}\,\boldsymbol{v}_s t - \mathrm{Ku}\,\mathrm{St}(\boldsymbol{v}_0 - \boldsymbol{v}_s)(e^{-t/\mathrm{St}} - 1). \tag{2}$$

Here $\boldsymbol{r}_0$ is the initial position of the particle, $\boldsymbol{v}_0$ is its initial velocity, and $\boldsymbol{v}_s \equiv F\mathrm{St}\hat{\boldsymbol{g}}$ is its settling velocity when $\boldsymbol{u} = 0$. The deviation $\delta\boldsymbol{r}_t \equiv \boldsymbol{r}_t - \boldsymbol{r}_t^{(d)}$ is given by the implicit solution of Eq. (1),

$$\delta\boldsymbol{r}_t = \frac{\mathrm{Ku}}{\mathrm{St}} \int_0^t dt_1 \int_0^{t_1} dt_2 e^{(t_2-t_1)/\mathrm{St}} \boldsymbol{u}(\boldsymbol{r}_{t_2}, t_2). \tag{3}$$

For small Ku the deviation $\delta\boldsymbol{r}_t$ is small and we expand the dynamics of $\mathbb{Z}$ and $\mathbb{A}$ in powers of $\delta\boldsymbol{r}_t$. This results in an expansion of $\mathrm{Tr}\mathbb{Z}$ in powers of Ku, expressed in terms of products of $\boldsymbol{u}(\boldsymbol{r}_t^{(d)},t)$ and its gradients. We compute the steady-state average $\langle \mathrm{Tr}\mathbb{Z}\rangle_\infty = \langle \nabla \cdot \boldsymbol{v}\rangle_\infty$ using the known statistics of $\boldsymbol{u}(\boldsymbol{r},t)$. To order Ku^3 we find

$$\begin{aligned}\langle \nabla \cdot \boldsymbol{v}\rangle_\infty = \frac{3\mathrm{Ku}^3}{4\mathrm{St}^5 G^8}\Big\{ & 2G^2\mathrm{St}^3[5 + 4\mathrm{St} + 3\mathrm{St}^2 - G^2\mathrm{St}^2(1+\mathrm{St})] + (1+\mathrm{St})^3[2(1+\mathrm{St})^2 - G^2\mathrm{St}^2(\mathrm{St}-3)]\mathcal{F}\left[\frac{1+\mathrm{St}}{\sqrt{2}\mathrm{St}G}\right]^2 \\ & - \sqrt{2}G\mathrm{St}^2[13 + 17\mathrm{St} + 15\mathrm{St}^2 + 3\mathrm{St}^3 + G^2\mathrm{St}^2(4 - \mathrm{St} - 3\mathrm{St}^2) + G^4\mathrm{St}^4]\mathcal{F}\left[\frac{1+\mathrm{St}}{\sqrt{2}\mathrm{St}G}\right] \\ & - 4G\mathrm{St}[1 + \mathrm{St}^2(2 + \mathrm{St}^2 + G^2)]\mathcal{F}\left[\frac{1}{G}\right] - 2\sqrt{\pi}(1+\mathrm{St}^2)G\{-2 + \mathrm{St}^2[-2 + (-3 + \mathrm{St}^2)G^2]\} \\ & \times \int_0^\infty dt \exp[G^{-2} - t/\mathrm{St} - G^2t^2/4]\mathrm{erfc}[G^{-1} + Gt/2]\Big\},\end{aligned} \tag{4}$$

where $\mathcal{F}[x] \equiv \sqrt{\pi}e^{x^2}\mathrm{erfc}(x)$ and $G \equiv \mathrm{Ku}\,\mathrm{St}\,F$ (Ku is small but G can take any value). Details are given in the Supplemental Material [33].

Preferential concentration.—A series expansion of Eq. (4) to lowest order in St with G treated as an independent parameter gives (see the Supplemental Material [33]),

$$\begin{aligned}\langle \nabla \cdot \boldsymbol{v}\rangle_\infty \sim\ & 3\mathrm{Ku}^3\mathrm{St}^2/(4G^5) \\ & \times \{4G - 6G^3 - (4 - 4G^2 + 3G^4)\mathcal{F}[G^{-1}]\}.\end{aligned} \tag{5}$$

Equation (5) describes preferential sampling due to the Maxey centrifuge effect. In the limit $G \to 0$ Eq. (5) approaches $\langle \nabla \cdot \boldsymbol{v}\rangle_\infty \sim -6\mathrm{Ku}^3\mathrm{St}^2$, see Ref. [14]. Expanding Eq. (4) for small values of G but arbitrary values of St yields

$$\begin{aligned}\langle \nabla \cdot \boldsymbol{v}\rangle_\infty = & -6\mathrm{Ku}^3\mathrm{St}^2\frac{1 + 3\mathrm{St} + \mathrm{St}^2}{(1+\mathrm{St})^3} + 9\mathrm{Ku}^3G^2\mathrm{St}^2 \\ & \times \frac{1 + 5\mathrm{St} + 12\mathrm{St}^2 + 20\mathrm{St}^3 + 4\mathrm{St}^4}{(1+St)^5} + \cdots.\end{aligned} \tag{6}$$

Equation (6) shows that gravitational settling reduces preferential sampling for all values of St provided G and Ku are small. We attribute this reduction to the fact that gravity causes the particles to fall through structures in the flow, rendering their preferential sampling less efficient. Finally, for large G and St Eq. (4) approaches

$$\langle \nabla \cdot \boldsymbol{v}\rangle_\infty \sim -3\sqrt{2\pi}\mathrm{Ku}^3\mathrm{St}/(4G^3). \tag{7}$$

The full analytical result (4) is compared to results of numerical simulations of Eq. (1) in Fig. 2(a). We observe good agreement except when G is small and St is large.

Preferential alignment.—Figure 1(b) shows vertically extended structures compared to the more isotropic structures in Fig. 1(a). We now show that this can be explained by the fact that the separation vector $\boldsymbol{R}$ between two nearby particles tends to align with $\pm\hat{\boldsymbol{g}}$ for large values of G. We characterize the alignment between $\boldsymbol{R}$ and $\hat{\boldsymbol{g}}$ by the moments $\langle(\hat{\boldsymbol{R}}\cdot\hat{\boldsymbol{g}})^{2p}\rangle_\infty$ for $p = 0, 1, \ldots$ and $\hat{\boldsymbol{R}} \equiv \boldsymbol{R}/|\boldsymbol{R}|$. Odd-order moments vanish. To find the even moments we use the small-Ku expansion described above. The expansion for $\hat{\boldsymbol{R}}$ contains secular terms as well as terms

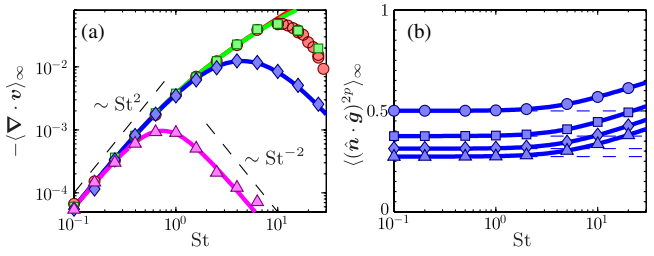

FIG. 2 (color online). Average divergence of particle velocity field $\langle\nabla\cdot\boldsymbol{v}\rangle_\infty$, and moments of the alignment $\langle(\hat{\boldsymbol{R}}\cdot\hat{\boldsymbol{g}})^{2p}\rangle$ between $\hat{\boldsymbol{R}}$ and $\hat{\boldsymbol{g}}$ shown as functions of St for Ku $= 0.1$. Markers show data from numerical simulations of Eq. (1). (a) Solid lines show Eq. (4). Dashed lines show the slopes of the asymptotes (5) with $G = 0$, and Eq. (7). Parameters: $F = 0$ (red, ○), $F = 0.1$ (green, □), $F = 1$ (blue, ◇), $F = 10$ (magenta, △). (b) Solid lines show results from the Padé-Borel resummation of Eq. (8) extended to order G^{78}; dashed lines show the isotropic result. Parameters: $F = 1$, $p = 1$ (○), $p = 2$ (□), $p = 3$ (◇), $p = 4$ (△).

depending on the initial configuration through $(\hat{\boldsymbol{R}}_0\cdot\hat{\boldsymbol{g}})^p$, $\boldsymbol{v}_0$, $\mathbb{Z}_0$, $\boldsymbol{u}_0$, and so forth. Requiring these terms to vanish (see the Supplemental Material [33]) yields a recursion which we solve as a power series in G. To fourth order in G

$$\langle(\hat{\boldsymbol{R}}\cdot\hat{\boldsymbol{g}})^{2p}\rangle_\infty = \frac{(2p-1)!!}{2^p p!}\left[1+\frac{pG^2}{p+1}-\frac{p(41+19p)G^4}{4(p+1)(p+2)}\right]. \quad (8)$$

When $G = 0$ the moments in Eq. (8) equal those of isotropically distributed orientation vectors $\hat{\boldsymbol{R}}$. For large values of G, $\langle(\hat{\boldsymbol{R}}\cdot\hat{\boldsymbol{g}})^{2p}\rangle_\infty$ increases: $\hat{\boldsymbol{R}}$ aligns with $\pm\hat{\boldsymbol{g}}$ because the matrix $\mathbb{Z}$ that changes the orientation of $\hat{\boldsymbol{R}}$ approximately follows an Ornstein-Uhlenbeck process with anisotropic driving. As $G\to\infty$ $\langle(\hat{\boldsymbol{R}}\cdot\hat{\boldsymbol{g}})^{2p}\rangle_\infty \to 1$ corresponding to complete alignment. We have obtained the expansion (8) to order 78 in G. The Padé-Borel resummation of this series yields results in excellent agreement with results from numerical simulations, Fig. 2(b).

Clustering of rapidly falling particles.—Particles with large settling speeds are insensitive to instantaneous fluid configurations. One might expect them to fall uniformly distributed. But Fig. 1(b) shows that rapidly falling particles may cluster despite the fact that they fall too fast to preferentially sample the flow. We quantify the degree of clustering by the spatial Lyapunov exponents

$$\lambda_1 \equiv \lim_{t\to\infty} t^{-1}\ln R_t, \qquad \lambda_1+\lambda_2 \equiv \lim_{t\to\infty} t^{-1}\ln \mathcal{A}_t, \quad (9)$$

the expansion (contraction) rates of the spatial distance $R_t \equiv |\boldsymbol{R}_t|$ between two initially nearby particles, and of the area element $\mathcal{A}_t$ spanned by the separation vectors between three nearby particles [9,11,13,34–36]. The Lyapunov exponents characterize the spatial distribution of the particles; they form a fractal with dimension [37]

$$d_L \equiv 2-(\lambda_1+\lambda_2)/\lambda_2 \quad (10)$$

(assuming $\lambda_1 > 0$ and $\lambda_1+\lambda_2 < 0$). We now show how to evaluate Eq. (10) in the limit of rapidly settling particles [Fig. 1(b)], assuming that $G \gg 1$. The deterministic settling trajectory (2) for large values of t is $\boldsymbol{r}_t^{(d)} = Gt$, and the particles experience rapid fluctuations of the flow velocity $\boldsymbol{u}(\boldsymbol{r}_t^{(d)}, t)$. The fluctuations decorrelate rapidly because particles fall many correlation lengths in a correlation time [38,39], and we find that the increments of the separation $\boldsymbol{R}$ and the relative velocity $\boldsymbol{V}$ between two nearby particles follow a Langevin equation,

$$\delta\boldsymbol{R} = \boldsymbol{V}'\delta t', \qquad \delta\boldsymbol{V}' = -\boldsymbol{V}'\delta t' + \delta\boldsymbol{F}. \quad (11)$$

Here we rescaled $t = t'\mathrm{St}$ and $\boldsymbol{v} = \boldsymbol{v}'/(\mathrm{Ku}\,\mathrm{St})$ as convenient in the white-noise limit [11–13,31]. Further $\delta\boldsymbol{F}$ is Gaussian white noise with zero mean and variance $\langle\delta F_i\delta F_j\rangle = 2\delta t'\mathrm{Ku}^2\mathrm{St}\sum_{kl}D_{ik,jl}R_kR_l$. The nonzero $D_{ik,jl}$ are given by

$$D_{21,21} = \frac{3}{\sqrt{8}G}\mathcal{F}\left[\frac{1}{\sqrt{2}G}\right], \qquad D_{12,12} = \frac{G^2-1}{2G^4}+\frac{D_{21,21}}{3G^4},$$
$$D_{11,11} = D_{22,22} = -D_{11,22} = -D_{22,11} = -D_{12,21}$$
$$= -D_{21,12} = \frac{1}{2G^2}-\frac{D_{21,21}}{3G^2}. \quad (12)$$

Since $D_{12,12} \neq D_{21,21}$ we see that gravity breaks isotropy, as discussed above. In Fig. 3(b) we show d_L obtained by numerical integration of Eqs. (11) and (12). We observe

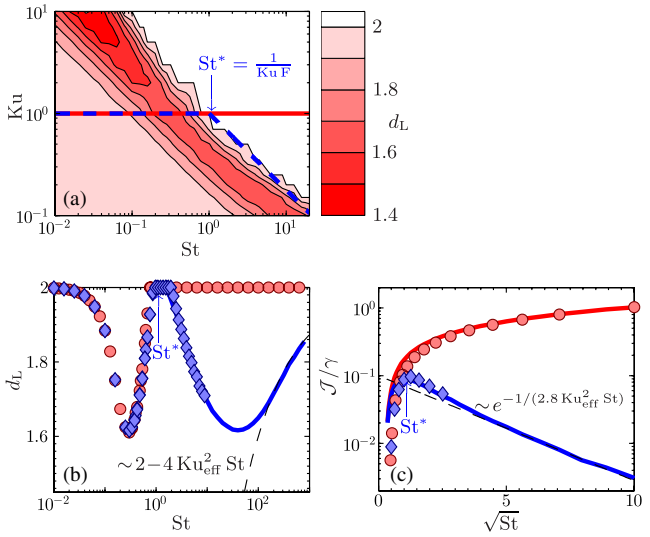

FIG. 3 (color online). Fractal dimension d_L and caustic formation rate $\mathcal{J}$ from numerical simulations of Eq. (1). (a) Contour plot of d_L as a function St and Ku for $F = 0$. Lines show $\mathrm{Ku}_{\mathrm{eff}}$, Eq. (13), as a function of St for $F = 0$ (solid red) and for $F = 1$ (dashed blue). (b) shows d_L and (c) shows $\mathcal{J}$ versus St with Ku $= 1$ for $F = 0$ (red, ∘) and $F = 1$ (blue, ◇). Black dashed lines show limiting behaviors for large G in terms of the parameter $\mathrm{Ku}_{\mathrm{eff}}^2\mathrm{St}$ with fitted prefactors. Solid lines show results of numerical integration of Eqs. (11) and (12).

strong clustering at large Stokes numbers, in good agreement with the results of direct numerical simulations of Eq. (1). This prediction is also borne out by recent results for the correlation dimension of particles falling through turbulence, obtained by direct numerical simulations [40]. For $F = 0$ inertial particles do not cluster at large St.

A qualitative explanation of this surprising phenomenon goes as follows. Figure 3(a) shows the degree of clustering as a function of St and Ku for $F = 0$. In this case, and for large values of St, the dynamics of $\mathbb{Z}$ is given by a single dimensionless parameter $\epsilon^2 \equiv \mathrm{Ku}^2\mathrm{St}/2$ [13]. Likewise, for the case of $F \neq 0$ with $G \gg 1$, the $\mathbb{Z}$ dynamics turns out to be governed by a single dimensionless parameter, obtained by a change of coordinates that diagonalizes the noise in Eq. (12). This parameter is $\epsilon^2/G^{3/2} = \sqrt{\mathrm{Ku}}/(2\sqrt{\mathrm{St}}F^{3/2})$, cf. the parameter dependence of Eq. (7): $\langle \nabla \cdot \boldsymbol{v}' \rangle_\infty \sim -3\sqrt{2\pi}(\epsilon^2/G^{3/2})^2$ [here $\boldsymbol{v}'$ is the particle velocity in the units used in Eq. (11)]. For a given value of St we map the $F > 0$ dynamics at large G onto the $F = 0$ dynamics by defining an effective Kubo number so that $\mathrm{Ku}_{\mathrm{eff}}^2\mathrm{St}/2 = \sqrt{\mathrm{Ku}}/(2\sqrt{\mathrm{St}}F^{3/2})$,

$$\mathrm{Ku}_{\mathrm{eff}} \sim \begin{cases} \mathrm{Ku} & \text{if } \mathrm{St} \ll \mathrm{St}^*, \\ \mathrm{Ku}^{1/4}/(F\mathrm{St})^{3/4} & \text{if } \mathrm{St} \gg \mathrm{St}^*. \end{cases} \tag{13}$$

Here $\mathrm{St}^* = 1/(\mathrm{Ku}F)$ is the scale at which the large-G asymptote meets the $G = 0$ asymptote.

Following the curve $\mathrm{Ku}_{\mathrm{eff}}$ for $\mathrm{Ku} = 1$ shown in Fig. 3(a), the clustering is approximately unmodified for $\mathrm{St} < \mathrm{St}^*$ [see Fig. 3(b)]. When $\mathrm{St} > \mathrm{St}^*$, $\mathrm{Ku}_{\mathrm{eff}}$ rapidly becomes so small that the curve reenters the region in parameter space where clustering occurs. In this limit the clustering is caused by many independent random accelerations ("multiplicative amplification") [14]; the instantaneous fluid configuration plays no role. For large F, the curve turns early and clustering may be small but nonzero for finite values of St [cf. $F = 1$ and $F = 10$ in Fig. 2(a)]. The fact that $\mathrm{Ku}_{\mathrm{eff}} \to 0$ as $\mathrm{F} \to \infty$ implies that spatial clustering disappears in the gravity-dominated limit. We remark that due to the anisotropy introduced by $\hat{\boldsymbol{g}}$, the matrix structure of the diffusion matrix Eq. (12) differs from that of the $F = 0$ case. This makes the mapping to the effective Ku number approximate.

Caustics.—When caustics are frequent, the expansion leading to Eq. (4) and related expansions in the white-noise limit do not converge, as seen in Fig. 2(a) for large values of St and $F = 0$ [11,13,14]. However, as shown in Fig. 3(c) for $\mathrm{St} > \mathrm{St}^*$ caustics are less frequent. For $F = 0$ the rate of caustic formation is of the form $\mathcal{J} \sim e^{-1/(3\mathrm{Ku}^2\mathrm{St})}$ in the white-noise limit provided that $\mathrm{Ku}^2\mathrm{St}$ is small [21]. It follows from Eq. (13) that caustics are deactivated when G becomes large, $e^{-1/(C\mathrm{Ku}_{\mathrm{eff}}^2\mathrm{St})}$. The constant C can be determined by a WKB approximation, but in Fig. 3(c) its value was fitted. We note that caustics are rare when St^* is so small that the curve in Fig. 3(a) turns before caustics are activated.

Conclusions.—We have derived a theory describing spatial clustering of particles falling through a turbulent flow, making it possible to determine how the clustering depends on the dimensionless parameters of the problem, F, St, and Ku. Our theory clearly demonstrates that the inertial response of the suspended particles to flow fluctuations and the effect of gravity are not additive.

For small and intermediate values of St, our theory shows that particles falling at finite F cluster less, because correlations between particles and flow structures are destroyed. This explains earlier DNS results [15–19].

For large values of St, our calculations show that settling particles may cluster strongly. This is surprising because for $F = 0$, particles are uniformly distributed at large Stokes numbers. Our theory shows that when the particles fall rapidly enough, they see the fluid gradients as a white-noise signal, giving rise to substantial clustering by the mechanism of multiplicative amplification, distinct from the mechanism causing clustering at small Stokes numbers (preferential concentration). This surprising result is consistent with the observations made in Ref. [19], but we note that in turbulent flows sweeping by large eddies may affect the dynamics of rapidly falling particles, and the clustering of rapidly falling particles may be modified by interactions with large eddies.

We find that for large values of St the spatial clustering is strongly anisotropic because the separation vector between two neighboring particles tends to align with $\pm\hat{\boldsymbol{g}}$. The Padé-Borel resummation of high-order perturbation theory allows us to quantify this anisotropy.

Finally, we find that the rate of caustic formation is reduced when St is large and F not too small. This implies smaller relative velocities between identical close-by particles, resulting in lower collision rates.

The problem of particles falling under gravity through a turbulent aerosol is important for rain initiation in warm turbulent rain clouds [29]. In this case the Stokes number takes values $\mathrm{St} \sim 10^{-3}(a/\mu\mathrm{m})^2$ [30]. The Stokes number increases as water droplets grow from $\mathrm{St} \sim 10^{-3}$ for small droplets (size 1 μm) to $\mathrm{St} \sim 10$ for large droplets (100 μm). In the absence of gravity in a flow with $\mathrm{Ku} \sim 1$, clustering is largest when St is of order unity. Typical values of the characteristic scales in vigorously turbulent rain clouds are $\tau \sim 10$ ms, $\eta \sim 1$ mm, and $u_0 \sim 0.1$ m/s [30], which gives Ku and F of order unity (blue curve in Fig. 3). Gravitational settling begins to become important for the motion of droplets larger than about 20 μm [41]. The corresponding Stokes number, $\mathrm{St} \sim 0.4$, is of the order of St^* [defined below Eq. (13)] for vigorously turbulent rain clouds. Our theory thus predicts that gravitational settling substantially changes the spatial clustering of rain droplets falling in turbulent rain clouds. This is expected to significantly increase the rate of turbulence-induced collision coalescence

of droplets of similar sizes, while the suppression of caustics at large St has the opposite effect.

Support by Vetenskapsrådet, by the Göran Gustafsson Foundation for Research in Natural Sciences and Medicine, and by C3SE and SNIC is gratefully acknowledged.

[1] E.-W. Saw, R. A. Shaw, S. Ayyalasomayajula, P. Y. Chuang, and A. Gylfason, Phys. Rev. Lett. **100**, 214501 (2008).
[2] J. Salazar, J. de Jonag, L. Cao, S. H. Woodward, H. Meng, and L. Collins, J. Fluid Mech. **600**, 245 (2008).
[3] M. Gibert, H. Xu, and E. Bodenschatz, J. Fluid Mech. **698**, 160 (2012).
[4] Z. Warhaft, Fluid Dyn. Res. **41**, 011201 (2009).
[5] J. Chun, D. L. Koch, S. L. Rani, A. Ahluwalia, and L. R. Collins, J. Fluid Mech. **536**, 219 (2005).
[6] J. Bec, L. Biferale, G. Boffetta, M. Cencini, S. Musacchio, and F. Toschi, Phys. Fluids **18**, 091702 (2006).
[7] E. Calzavarini, M. Cencini, D. Lohse, and F. Toschi, Phys. Rev. Lett. **101**, 084504 (2008).
[8] E. Meneguz and M. Reeks, J. Fluid Mech. **686**, 338 (2011).
[9] J. Bec, Phys. Fluids **15**, L81 (2003).
[10] M. R. Maxey, J. Fluid Mech. **174**, 441 (1987).
[11] K. Duncan, B. Mehlig, S. Östlund, and M. Wilkinson, Phys. Rev. Lett. **95**, 240602 (2005).
[12] B. Mehlig, M. Wilkinson, K. Duncan, T. Weber, and M. Ljunggren, Phys. Rev. E **72**, 051104 (2005).
[13] M. Wilkinson, B. Mehlig, S. Östlund, and K. P. Duncan, Phys. Fluids **19**, 113303(R) (2007).
[14] K. Gustavsson and B. Mehlig, Europhys. Lett. **96**, 60012 (2011).
[15] G. Falkovich and A. Pumir, Phys. Fluids **16**, L47 (2004).
[16] L. Wang, O. Ayala, Y. Xue, and W. Grabowski, J. Atmos. Sci. **63**, 2397 (2006).
[17] C. Franklin, P. Vaillancourt, and M. Yau, J. Atmos. Sci. **64**, 938 (2007).
[18] O. Ayala, B. Rosa, L.-P. Wang, and W. Grabowski, New J. Phys. **10**, 075015 (2008).
[19] E. Woittiez, H. Jonker, and L. Portela, J. Atmos. Sci. **66**, 1926 (2009).
[20] The parameter F is referred to as the "Froude number" by R. A. Shaw in Annu. Rev. Fluid Mech. **35**, 183 (2003). But there are many different conventions in the literature. A common one is to define the Froude number as $\boldsymbol{F}^{-1}$; see, for example, B. J. Devenish *et al.*, Q. J. R. Meteorol. Soc. **138**, 1401 (2012).
[21] M. Wilkinson, and B. Mehlig, Europhys. Lett. **71**, 186 (2005).
[22] M. Wilkinson, B. Mehlig, and V. Bezuglyy, Phys. Rev. Lett. **97**, 048501 (2006).
[23] G. Falkovich, A. Fouxon, and G. Stepanov, Nature (London) **419**, 151 (2002).
[24] J. Bec, L. Biferale, M. Cencini, A. Lanotte, and F. Toschi, J. Fluid Mech. **646**, 527 (2010).
[25] K. Gustavsson and B. Mehlig, Phys. Rev. E **84**, 045304 (2011).
[26] J. Salazar and L. Collins, J. Fluid Mech. **696**, 45 (2012).
[27] G. P. Bewley, E. W. Saw, and E. Bodenschatz, New J. Phys. **15**, 083051 (2013).
[28] K. Gustavsson and B. Mehlig, J. Turbul. **15**, 34 (2014).
[29] B. J. Devenish *et al.*, Q. J. R. Meteorol. Soc. **138**, 1401 (2012).
[30] R. A. Shaw, Annu. Rev. Fluid Mech. **35**, 183 (2003).
[31] K. Gustavsson and B. Mehlig, Phys. Rev. E **87**, 023016 (2013).
[32] K. Gustavsson, J. Einarsson, and B. Mehlig, Phys. Rev. Lett. **112**, 014501 (2014).
[33] See Supplemental Material at http://link.aps.org/supplemental/10.1103/PhysRevLett.112.214501 for a summary of the method used to derive Eq. (4).
[34] J. Sommerer and E. Ott, Science **259**, 335 (1993).
[35] M. Wilkinson and B. Mehlig, Phys. Rev. E **68**, 040101(R) (2003).
[36] B. Mehlig and M. Wilkinson, Phys. Rev. Lett. **92**, 250602 (2004).
[37] J. Kaplan and J. A. Yorke, Lect. Notes Math. **730**, 204 (1979).
[38] V. Bezuglyy, B. Mehlig, M. Wilkinson, K. Nakamura, and E. Arvedson, J. Math. Phys. (N.Y.) **47**, 073301 (2006).
[39] I. Fouxon, and P. Horvai, Phys. Rev. Lett. **100**, 040601 (2008).
[40] J. Bec, H. Hohmann, and S. Sankar Ray, arXiv:1401.1306.
[41] P. R. Jonas, Atmos. Res. **40**, 283 (1996).